doi:10.1093/jmcb/mjz107
Published online December 21, 2019

Article

Methylation of PLK1 by SET7/9 ensures accurate kinetochore–microtubule dynamics

Ruoying Yu[1,3,†], Huihui Wu[1,3,†], Hazrat Ismail[1,2], Shihao Du[1,2,3], Jun Cao[1], Jianyu Wang[1], Tarsha Ward[1,2,3,4], Fengrui Yang[1,2], Ping Gui[1,2,3], Mahboob Ali[1,2], Lingluo Chu[1,4], Fei Mo[1,4], Qi Wang[5], Youjun Chu[1,3], Jianye Zang[1], Yun Zhao[1,6], Mingliang Ye[5], Guowei Fang[1], Peng R. Chen[7], Zhen Dou[1,3], Xinjiao Gao[1,*], Wenwen Wang[1,3,*], Xing Liu[1,3,*], and Xuebiao Yao[1]

[1] MOE Key Laboratory for Cellular Dynamics & Anhui Key Laboratory for Chemical Biology, CAS Center for Excellence in Molecular Cell Science, Hefei National Science Center for Physical Sciences at Microscale & University of Science and Technology of China, Hefei 230027, China
[2] BUCM-MSM-USTC Joint Program on Global Health Equity, Beijing University of Chinese Medicine, Beijing 100029, China
[3] Department of Physiology, Morehouse School of Medicine, Atlanta, GA 30310, USA
[4] Harvard Medical School, Boston, MA 02115, USA
[5] Dalian Institute for Physical Chemistry, Dalian 116023, China
[6] Shanghai Institute of Biochemistry and Cell Biology, Center for Excellence in Molecular Cell Science, Chinese Academy of Sciences, Shanghai 200031, China
[7] College of Chemistry and Molecular Engineering, Peking University, Beijing 100871, China
[†] These authors contributed equally to this work.
[*] Correspondence to: Xing Liu, E-mail: xing1017@ustc.edu.cn; Wenwen Wang, E-mail: wwwang@ustc.edu.cn; Xinjiao Gao, E-mail: gaox@ustc.edu.cn

Edited by Zhiyuan Shen

Faithful segregation of mitotic chromosomes requires bi-orientation of sister chromatids, which relies on the sensing of correct attachments between spindle microtubules and kinetochores. Although the mechanisms underlying PLK1 activation have been extensively studied, the regulatory mechanisms that couple PLK1 activity to accurate chromosome segregation are not well understood. In particular, PLK1 is implicated in stabilizing kinetochore–microtubule attachments, but how kinetochore PLK1 activity is regulated to avoid hyperstabilized kinetochore–microtubules in mitosis remains elusive. Here, we show that kinetochore PLK1 kinase activity is modulated by SET7/9 via lysine methylation during early mitosis. The SET7/9-elicited dimethylation occurs at the Lys191 of PLK1, which tunes down its activity by limiting ATP utilization. Overexpression of the non-methylatable PLK1 mutant or chemical inhibition of SET7/9 methyltransferase activity resulted in mitotic arrest due to destabilized kinetochore–microtubule attachments. These data suggest that kinetochore PLK1 is essential for stable kinetochore–microtubule attachments and methylation by SET7/9 promotes dynamic kinetochore–microtubule attachments for accurate error correction. Our findings define a novel homeostatic regulation at the kinetochore that integrates protein phosphorylation and methylation with accurate chromosome segregation for maintenance of genomic stability.

Keywords: mitosis, PLK1 kinase, SET7/9, methylation, kinetochore–microtubule attachment

Introduction

The kinetochore is a membraneless organelle assembled at eukaryotic chromosome centromere, which provides a chromosomal attachment point for the mitotic spindle, linking the chromosome to the microtubules and functions in controlling and guiding chromosome movements during mitosis. Proper bi-orientation of chromosomes is critical for the accurate segregation of chromosomes, which in turn is essential for maintaining genomic integrity (Rajagopalan and Lengauer, 2004). However, the molecular mechanisms underlying epigenetic regulation of centromere plasticity and genomic stability have remained elusive (Cleveland et al., 2003). Mounting evidence demonstrates that the master mitotic kinase CDK1 together with PLK1, Aurora kinases, and the NIMA-related kinases orchestrate the chromosome segregation in mitosis (Ke et al., 2003; Yang et al., 2008; Zhang et al., 2011; Duan et al., 2016) PLK1 is an important kinase that orchestrates this process and involved in the regulation of centrosome

Received September 11, 2019. Revised November 5, 2019. Accepted November 11, 2019.

maturation, mitotic entry, checkpoint recovery, spindle assembly, sister chromatid separation, and even cytokinesis. From G2 phase to mitosis, PLK1 is localized at centrosome. During mitosis, PLK1 is accumulated at kinetochores from prophase to metaphase, and subsequently translocates to midzone in anaphase (Golsteyn et al., 1995; Takaki et al., 2008). Both protein level and kinase activity of PLK1 are strictly regulated through mitosis. Accordingly, PLK1 function depends on its subcellular localization. Persistent localization of PLK1 to kinetochores at metaphase led to reduced inter-kinetochore tension and intra-kinetochore stretch, a checkpoint-dependent mitotic arrest, and accumulation of erroneous kinetochore-microtubule attachments (Liu et al., 2012), suggesting that kinetochore PLK1 activity and its signaling events are precisely regulated to avoid hyperstabilized kinetochore-microtubule attachments. Despite our early demonstration of regulation of PLK1 signaling cascade at the kinetochore (Zhang et al., 2011), it still remains poorly illustrated how kinetochore PLK1 activity is regulated during mitosis. Specifically, little is known about whether phosphorylation cascades crosstalk with other post-translational modifications such as methylation at the kinetochore during chromosome segregation in mitosis.

The methylation of histone H3 on lysine 9 is a hallmark of heterochromatin establishment in most eukaryotes and serves as a binding site for HP1 family proteins, which play critical roles in maintaining chromatin structure and ensuring faithful chromosome segregation during cell division (Chu et al., 2012; Akram et al., 2018). Methylation of non-histone proteins such as tubulin serves as a 'code' that fine-tunes the genomic stability (Park et al., 2016). Methylation is mediated by methyltransferase, such as SET7/9, a typical member of the family of non-chromatin lysine methyltransferases (KMTase) (Nishioka et al., 2002). SET7/9 transfer methyl groups to lysine residues to generate a mono- or dimethyl mark (Huang et al., 2006). The non-histone substrates of SET7/9, including p53 (Campaner et al., 2011), E2F1 (Kontaki and Talianidis, 2010), and DNMT1 (Esteve et al., 2009), regulate cell division cycle.

Here, we identified a novel molecular mechanism regulating kinetochore–microtubule dynamics by SET7/9-elicited methylation in mitosis. We found that SET7/9 is a binding protein for PLK1 *in vitro* and *in vivo*. Interestingly, SET7/9 methylates PLK1 and inhibits its kinase activity by limiting its access to ATP. Using a fluorescence resonance energy transfer (FRET)-based PLK1 kinase sensor in live cell, our quantitative analysis revealed that the temporal dynamics of kinetochore PLK1 activity is regulated by SET7/9 during chromosome segregation. Our study suggested that SET7/9 methyl-transferase activity orchestrates kinetochore-microtubule dynamics via a novel methylation-phosphorylation signaling crosstalk.

Results

SET7/9 is required for faithful chromosome progression

To explore potential regulators that govern kinetochore PLK1 activity and delineate the molecular function of PLK1 during early mitosis, we carried out mass spectrometric analysis of prometaphase-synchronized HeLa cells and uncovered several potential PLK1 interacting proteins (Supplementary Figure S1A, lane 2). One of top hits reproducibly identified by mass spectrometric analyses was SET7/9 methyltransferase that catalyzes lysine methylation of histone and non-histone proteins (Fu et al., 2016). To evaluate the function of SET7/9 in mitosis, we employed two independent siRNAs to suppress the endogenous SET7/9 in cultured HeLa cells and examined the resulting mitotic phenotype using time-lapse microscopy (Figure 1A). In general, these two independent siRNAs exhibit typical depletion of 85% ± 5% of endogenous proteins judged by western blotting analyses (Figure 1B; Supplementary Figure S1B). Whereas cells treated with control siRNA progressed normally through mitosis, SET7/9-suppressed cells showed a high frequency of chromosome segregation defects, including anaphase lagging chromosomes, chromosome misalignment and chromosome bridges (Figure 1A and C–E). The defects seen in the SET7/9-deficient cells were common phenotypes from two independent siRNAs and largely rescued by expressing an RNA interference (RNAi)-resistant, wild-type SET7/9, but not with an methyltransferase-deficient form of SET7/9 (data not shown), demonstrating the role of SET7/9 methyltransferase activity in accurate chromosome movements during mitosis.

To rule out the possibility that the phenotype was a consequence of disruption of SET7/9 function in the DNA Damage response pathway (Wang et al., 2009), we introduced two small-molecule inhibitors of SET7/9 methyltransferase with distinctly different mechanisms of action, PFI-2 (Barsyte-Lovejoy et al., 2014) and cyproheptadine (Hirano et al., 2018), into cultured cells immediately after mitotic entry. As expected, chemical inhibition of SET7/9 methyltransferase activity using two structurally independent compounds resulted in increased rates of chromosome misalignment and mis-segregation (Figure 1F–H). Thus, SET7/9 methyltransferase activity was essential for chromosome alignment and accurate metaphase-anaphase transition.

PLK1 is a cognate substrate of SET7/9 in vitro and in vivo

Lysine methylation is an important post-translational modification that regulates cellular plasticity (Fu et al., 2016). However, no evidence shows the relationship between SET7/9 and PLK1 in cell division control. To delineate the mechanism of action underlying SET7/9 function relative to PLK1 in mitosis, we first examined their biochemical interaction in mitotic cells. To this end, we performed immunoprecipitation assays, in which HeLa cells were synchronized in prometaphase of mitosis using nocodazole. The synchronized cells were then lysed and incubated with an anti-PLK1 antibody coupled affinity matrix to isolate PLK1 and its accessory proteins. As shown in Figure 2A, the outcome of immunoblotting analysis using an anti-SET7/9 antibody confirmed that SET7/9 was brought down by PLK1 antibody (lane 3) but not control IgG (lane 4). The association of PLK1 with SET7/9 was further confirmed by a co-immunoprecipitation experiment in which HEK293T cells were transiently co-transfected to express FLAG-PLK1 and GFP-SET7/9 (Figure 2B, lane 4).

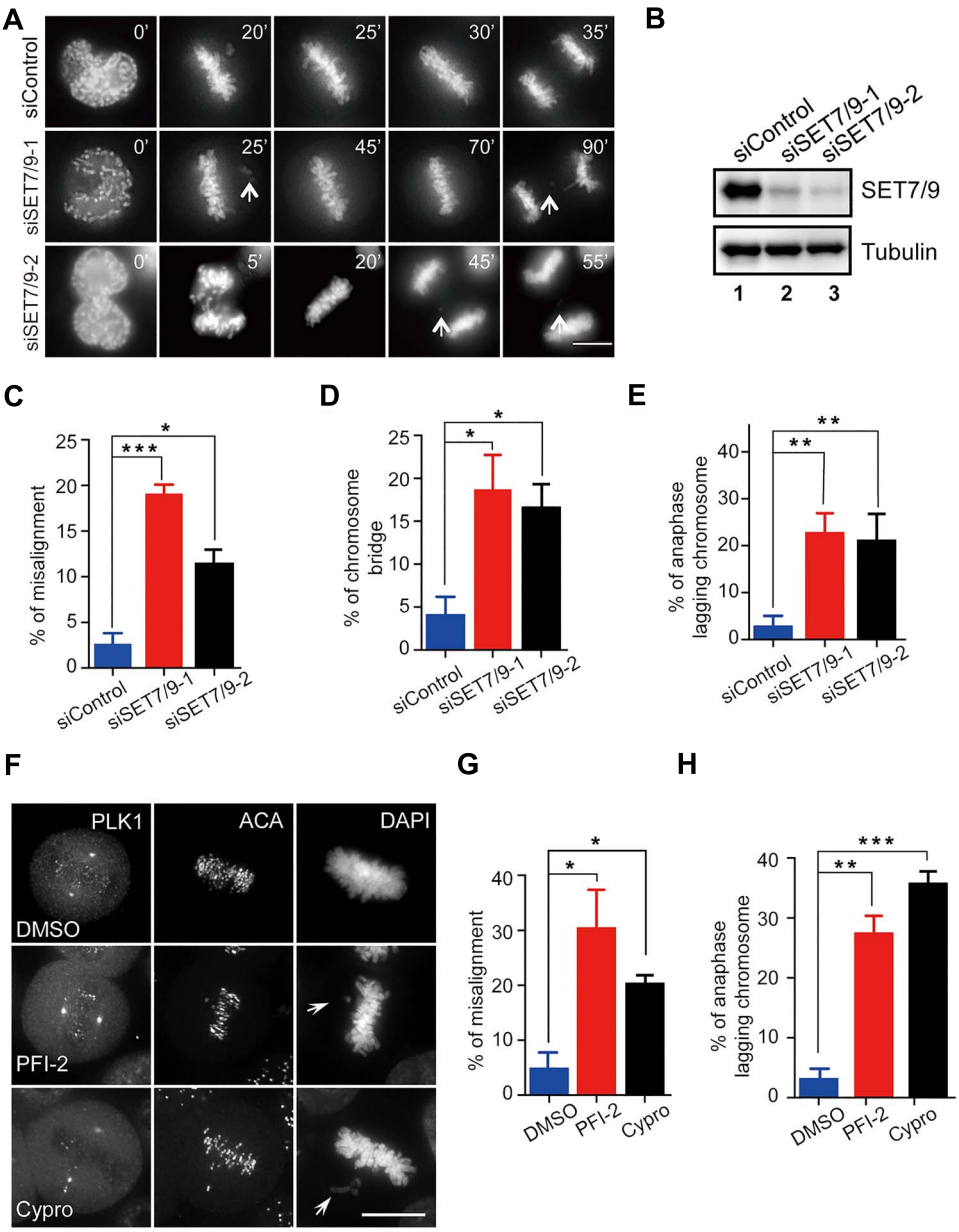

Figure 1 SET7/9 is required for accurate chromosome segregation. (**A**) Representative mitotic phenotypes in HeLa cells transfected with SET7/9 or control siRNA. Arrows, misaligned/lagging chromosomes; numbers at bottom left of images indicate elapsed time in minutes. Scale bar, 10 μm. (**B**) Representative western blotting analysis of SET7/9 siRNA-mediated knockdown efficiency for real-time imaging experiment shown in **A**. (**C**–**E**) Quantification of mitotic phenotypes of live HeLa cells transfected with control (n = 108) or SET7/9 siRNAs (n = 99, siRNA-1; n = 101, siRNA-2). Cells exhibiting unaligned chromosomes and failing to align at the metaphase plate within 60 min after nuclear envelope breakdown were considered to be misaligned (**C**). Data represent mean ± SEM from three independent experiments. (**F**) Representative mitotic phenotypes in HeLa cells treated with DMSO, PFI-2 (10 μM), or cyproheptadine (2 μM). HeLa cells were treated with DMSO, PFI-2 (10 μM), or cyproheptadine (2 μM) in the presence of MG132 for 1 h after 8 h release from thymidine arrest. Cells were fixed and stained with the indicated antibodies as illustrated. Scale bar, 10 μm. (**G** and **H**) Quantification of mitotic phenotypes in **F**. Data represent mean ± SEM from three independent experiments of > 100 cells. Statistical significance was tested by two-sided t-test; *$P < 0.05$, **$P < 0.01$, ***$P < 0.001$.

To examine whether PLK1 directly binds to SET7/9, we carried out pull-down assay in which GST-SET7/9 was used as affinity matrix and His-PLK1 was apparently retained on GST-SET7/9 (Figure 2C, lane 3), but not GST affinity matrix (Figure 2C, lane 2). We next sought to pinpoint which functional domain of PLK1 locates to the interacting interface of PLK1–SET7/9. Interestingly, only PLK1 full-length ($PLK1^{FL}$) binds with SET7/9 (Supplementary Figure S2A, lane 4).

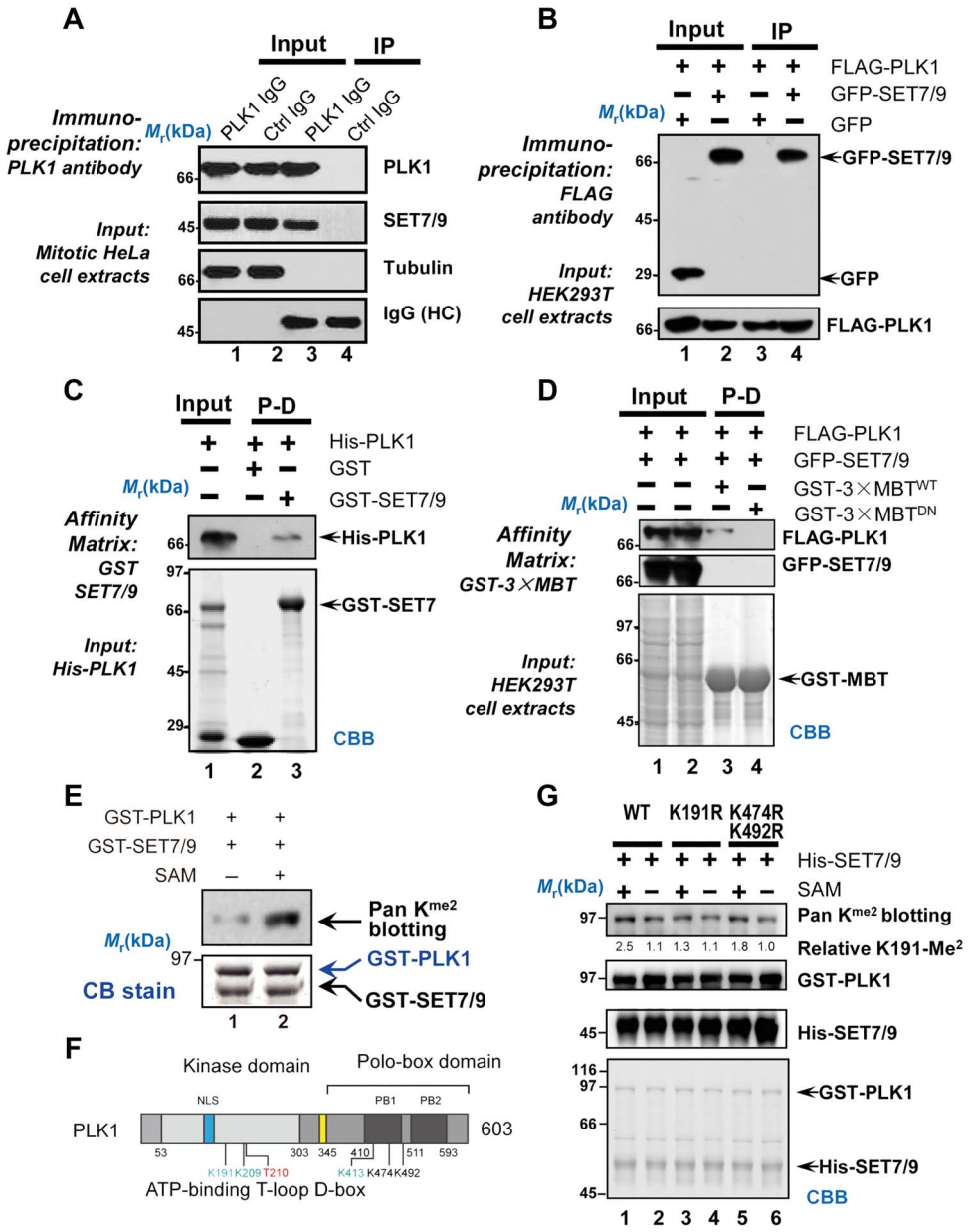

Figure 2 PLK1 is a cognate substrate of SET7/9 *in vitro* and *in vivo*. (**A**) Immunoprecipitation of endogenous PLK1 from prometaphase-synchronized HeLa cells. Clarified extracts from mitotic HeLa cells were incubated with an anti-PLK1 antibody and immunoprecipitates were resolved by SDS–PAGE followed by western blotting analyses using indicated antibodies. (**B**) Immunoprecipitation of FLAG-PLK1 from HEK293T cells co-transfected with GFP or GFP-SET7/9. The immunoprecipitates were analyzed by an anti-GFP western blotting. (**C**) Recombinant GST-SET7/9 or GST proteins were incubated with His-PLK1 for 4 h, and their interactions were assessed by Coomassie Brilliant Blue (CBB)-stained SDS–PAGE gel and western blot with an anti-His antibody blotting analysis. (**D**) GST-3×MBT^{WT} and GST-3×MBT^{DN} bound agarose beads were used as affinity matrices to absorb methylated PLK1 from HEK293T cells co-transfected with FLAG-PLK1 and GFP-SET7/9. (**E**) Aliquots of purified GST-PLK1 were incubated with 0.5 μg GST-SET7/9 in the presence or absence of 1 mM S-(5′-adenosyl)-Lmethionine (SAM). PLK1 methylation was detected by dimethyl lysine antibody. Methylated lysine residues in PLK1 from *in vitro* methylation reaction were identified using mass spectrometric analysis. (**F**) Diagram of PLK1 functional domains relative to newly identified lysine residues bearing methylation. (**G**) Characterization of K191 methylation *in vitro*. Aliquots of purified GST-PLK1 and GST-PLK1 mutants (K191R and K474R/K492R; 0.5 μg) were incubated with 0.5 μg of His-SET7/9 in the presence or absence of 1 mM SAM. Methylated PLK1 was detected by western blotting analyses using an anti-dimethyl lysine antibody.

As a specific reader, three malignant brain tumor repeats (3× MBT hereafter) bind to mono- or dimethylated lysine residue with remarkable specificity (Kalakonda et al., 2008). The specific binding of 3× MBT to mono- or dimethylated lysine requires a conserved aspartic acid (D355) in the second MBT repeat as D355 mutation (D355N) disrupts 3× MBT binding to mono- or

dimethylated lysine. Thus, D355 mutated 3× MBT (3× MBT^{D355N}) was used as a negative control for 3× MBT affinity pull-down. To examine whether PLK1 is methylated by SET7/9, GST-3×MBT^{WT} (wild type) and GST-3×MBT^{DN} (D355N) were used as affinity matrices to isolate PLK1 from HEK293T cells expressing FLAG-PLK1 and GFP-SET7/9. Consistent with prediction, FLAG-PLK1 was retained on GST-3×MBT^{WT} but not GST-3×MBT^{DN} affinity matrix (Figure 2D, lane 3 vs. lane 4). Using a pan dimethyl lysine (Pan K^{me2}) antibody, western blotting analyses showed that PLK1 is methylated (Figure 2E, top panel, lane 2). To pinpoint which domain(s) of PLK1 are methylated, a 3× MBT pull-down assay was conducted. To our surprise, the kinase domain of PLK1 contains methylated lysine residues (Supplementary Figure S2B, lane 6).

To identify methylated lysine residues, PLK1 protein isolated from *in vitro* methylation assay was subjected to mass spectrometry analyses. As a result, we identified a total of three dimethylated lysine sites including K191, K474 and K492 (Figure 2E and F), but not mono- or tri-methylated on PLK1. To confirm these sites responsible for SET7/9 methylation, we generated a series of PLK1 mutants in which three identified methylation sites were individually mutated to arginine. As shown in Figure 2G, methylation of PLK1 mutants (K191R; K474/492R) was significantly reduced compared with PLK1^{WT}, indicating that Lys191, Lys474, and Lys492 are substrates of SET7/9. Importantly, our mass spectrometric analysis of endogenous PLK1 isolated from mitotic HeLa cells confirmed that K191 of PLK1 was dimethylated (Supplementary Figure S2C), suggesting that Lys191 of PLK1 is a physiological substrate of SET7/9 in mitosis. Significantly, our computational analyses demonstrate that Lys191 is evolutionarily conserved from yeast to human (Supplementary Figure S3), suggesting a functional conservation of Lys191 and its regulatory mechanisms in eukaryotic kingdom.

PLK1 K191 is methylated during late G2 phase and mitosis

To characterize the spatiotemporal dynamics of PLK1 methylation, we generated a site-specific dimethylation antibody, K191^{me2}. The specificity of this antibody was confirmed by western blotting analysis using the extracts of HEK293T cells co-transfected with GFP-SET7/9 and FLAG-PLK1^{WT} or FLAG-PLK1^{K191R}. As shown in Figure 3A, this antibody exhibits selective reactivity to methylated PLK1 (lane 1) but not non-methylatable PLK1 (PLK1^{K191R}). The total protein levels of FLAG-PLK1^{WT} and FLAG-PLK1^{K191R} are comparable judged by immunoblotting assay (Figure 3A, lower panel). To assess whether Lys191 of PLK1 is a cognate substrate of SET7/9 in mitosis, we analyzed Lys191 methylation in aliquots of unsynchronized HeLa cells. Lys191 methylation was dramatically reduced after SET7/9 depletion (Supplementary Figure S4A, lanes 2 and 3), indicating that Lys191 is a cognate substrate of SET7/9.

To determine the temporal dynamics of Lys191 methylation during cell cycle, aliquots of synchronized HeLa cells were collected at indicated intervals after release from the G1/S phase and subjected to western blotting analyses. As shown in Figure 3B, PLK1 methylation was analyzed by immunoblotting with K191^{me2} antibody. Cyclin B1 accumulation (6 h after release) marked advance into the G2 phase and was sustained until anaphase onset (10 h after release), consistent with previous studies (Mo et al., 2016; Huang et al., 2019). PLK1-K191^{me2} appeared after the rise of cyclin B1, and was sustained beyond anaphase entry when cyclin B1 level declined (10 h after release, Figure 3B), demonstrating that the Lys191 methylation is temporally independent of CDK1–cyclin B1. Despite our detection of a cyclic profile of BubR1, the phosphorylation-elicited mobility shift of BubR1 was not apparent in our analyses (Figure 3B, top panel), which is consistent with the literature (Seki et al., 2008; Liu et al., 2012). We next sought to examine the level of K191^{me2} in mitosis and compare it with that of interphase. Our western blotting analyses of PLK1 isolated from interphase and mitosis demonstrated that the level of K191^{me2} is ∼2.7-fold higher in mitosis compared to that of G2 cells (Figure 3C). Since PLK1 is localized at kinetochore and centrosome in mitotic cells, we next examined the localization of K191^{me2} relative to PLK1 protein in mitotic cells. As shown in Figure 3D, immunofluorescence microscopic analyses showed that signal of K191^{me2} was present at metaphase kinetochores superimposed onto these of PLK1 in mitotic cells and their co-localization to the kinetochore was persistent even until anaphase B. As the function of PLK1 in mitosis is elicited by Aurora A phosphorylation of Thr210 (pT210), we next examined the subcellular distribution profile of pT210-PLK1 relative to K191^{me2}. As shown in Figure 3E, the signal of pT210 is superimposed onto that of K191^{me2} in metaphase HeLa cells, suggesting that Lys191 methylation is parallel to that of pT210-PLK1 in mitotic cells. Thus, Lys191 methylation is a physiological substrate of SET7/9 during mitosis.

Lys191 methylation by SET7/9 suppresses PLK1 kinase activity

Because Lys191 is evolutionarily conserved in eukaryotic kingdom and its position is close to the ATP pocket of PLK1 (as shown in Supplementary Figure S3B), we hypothesized that methylation of Lys191 by SET7/9 may regulate PLK1 activity. Given the fact that PLK1 activation involves in Aurora A-mediated phosphorylation of Thr210, we sought to test whether SET7/9 methylates PLK1 in the presence of phosphorylated Thr210. As shown in Figure 4A, Aurora A phosphorylated PLK1 at Thr210 in the presence of Bora (lane 2). As predicted, addition of SET7/9 resulted in methylated PLK1 in the presence of SAM (lane 3) judged by K191^{me2} antibody. To assess whether methylation of PLK1 at Lys191 regulates its kinase activity, we carried out an *in vitro* kinase assay using a fluorimetric kinase assay kit (Mo et al., 2016; Huang et al., 2019). Specifically, we purified GST-PLK1 from *Escherichia coli* and subjected it to Aurora A phosphorylation prior to an *in vitro* methylation with His-SET7/9. As predicted and shown in Figure 4B, Aurora A robustly stimulated PLK1 activity in an ATP-dependent manner (green line). Surprisingly, treatment of PLK1 with SET7/9 diminished the PLK1 activity

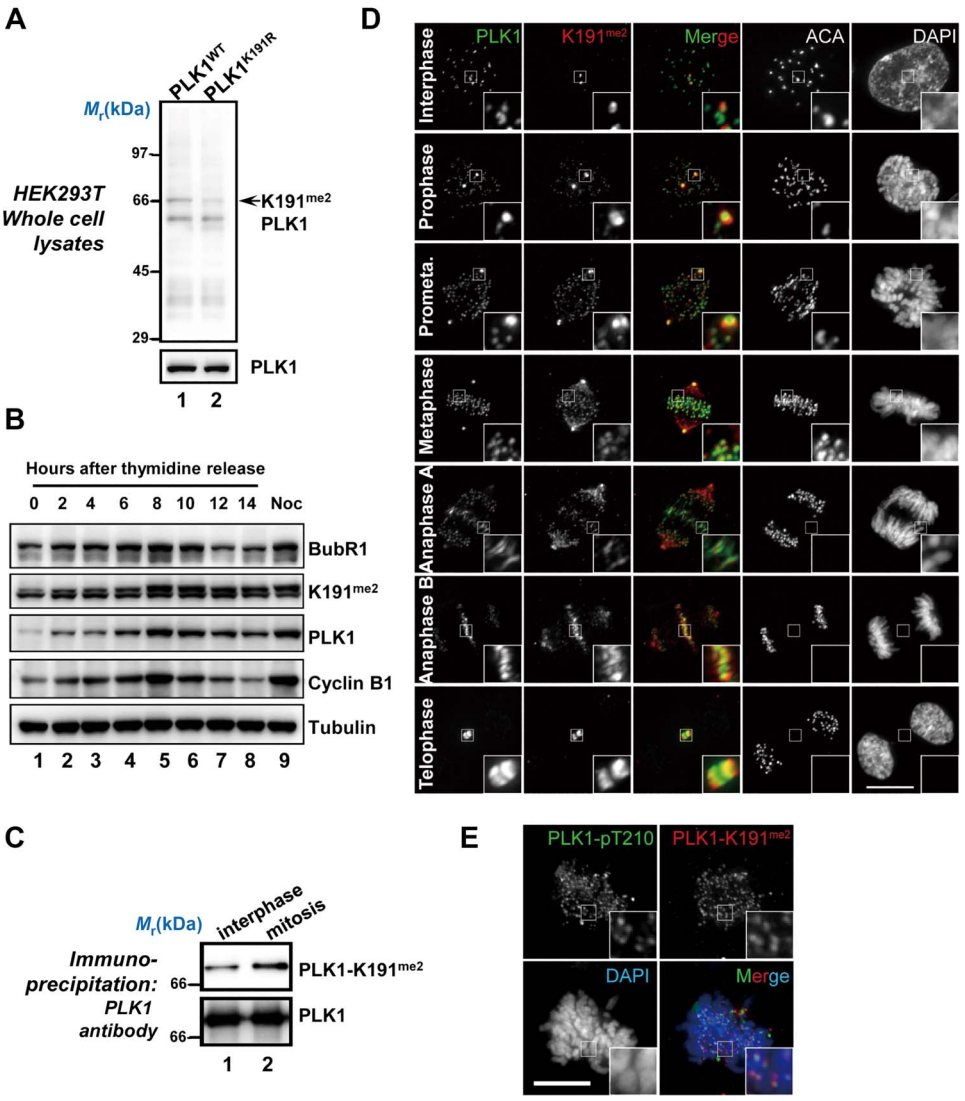

Figure 3 PLK1 K191 is methylated during G2 phase and mitosis. (**A**) Characterization of the specificity of the PLK1-K191^{me2} antibody. HEK293T cells were co-transfected with GFP-SET7/9 and FLAG-Plk1^{WT} or FLAG-PLK1^{K191R} followed by western blotting analyses of PLK1 and PLK1-K191^{me2}, respectively. (**B**) HeLa cells were arrested by nocodazole or synchronized to the indicated time points by double thymidine release and probed for PLK1-K191^{me2} and other indicated proteins. (**C**) Immunoprecipitation of endogenous PLK1 from asynchronized or nocodazole-synchronized HeLa cells. HeLa cell extracts were incubated with an anti-PLK1 antibody. After extensive washes, immunoprecipitates were resolved by SDS–PAGE followed by western blotting analyses using indicated antibodies. The methylation level of PLK1 was detected by PLK1-K191^{me2} antibody. (**D**) Representative immunofluorescence staining of PLK1 and PLK1-K191^{me2} in HeLa cells at different mitotic stages. Scale bar, 10 μm. (**E**) Co-localization analysis of K191-methylated (K191^{me2}) and Thr210-phosphorylated (pT210) PLK1 at prometaphase kinetochores in HeLa cells. Scale bar, 10 μm.

pre-activated by Aurora A (blue line), suggesting that methylation of PLK1 by SET7/9 perhaps interfered with the access of substrates such as ATP to the activated kinase. To assess the impact of K191 methylation on PLK1 kinase activity, we measured the kinetics of ATP catalyzed by FLAG-PLK1^{WT} and FLAG-PLK1^{K191R}, respectively. As shown in Supplementary Figure S5A, the k_{cat}/K_m ratio changed by 4-fold (from 0.3 to 1.2) when ATP was used as a substrate in a dose-responsive study. Interestingly, the k_{cat}/K_m ratio only changed 2-fold (from 2.2 to 4.9) when Cep55 peptide was used as a substrate. The enzymatic assays suggest that utilization of ATP is limited by PLK1 methylation in kinetic reaction. To test our hypothesis whether dimethylation of PLK1 at Lys191 suppresses its kinase activity through impairing the utility of ATP, we used ATP coupled agarose beads as affinity matrix to absorb the FLAG-PLK1^{WT} or FLAG-PLK1^{K191R} purified from HEK293T cells transiently co-transfected with GFP-SET7/9 and FLAG-PLK1^{WT} or FLAG-PLK1^{K191R}. As shown in Figure 4C, ATP matrix retained a higher level of FLAG-PLK1^{K191R} than FLAG-PLK1^{WT}, suggesting that K191 methylation may weaken its ATP binding ability. Using molecular modeling illustrated in Figure 4D, we reasoned that

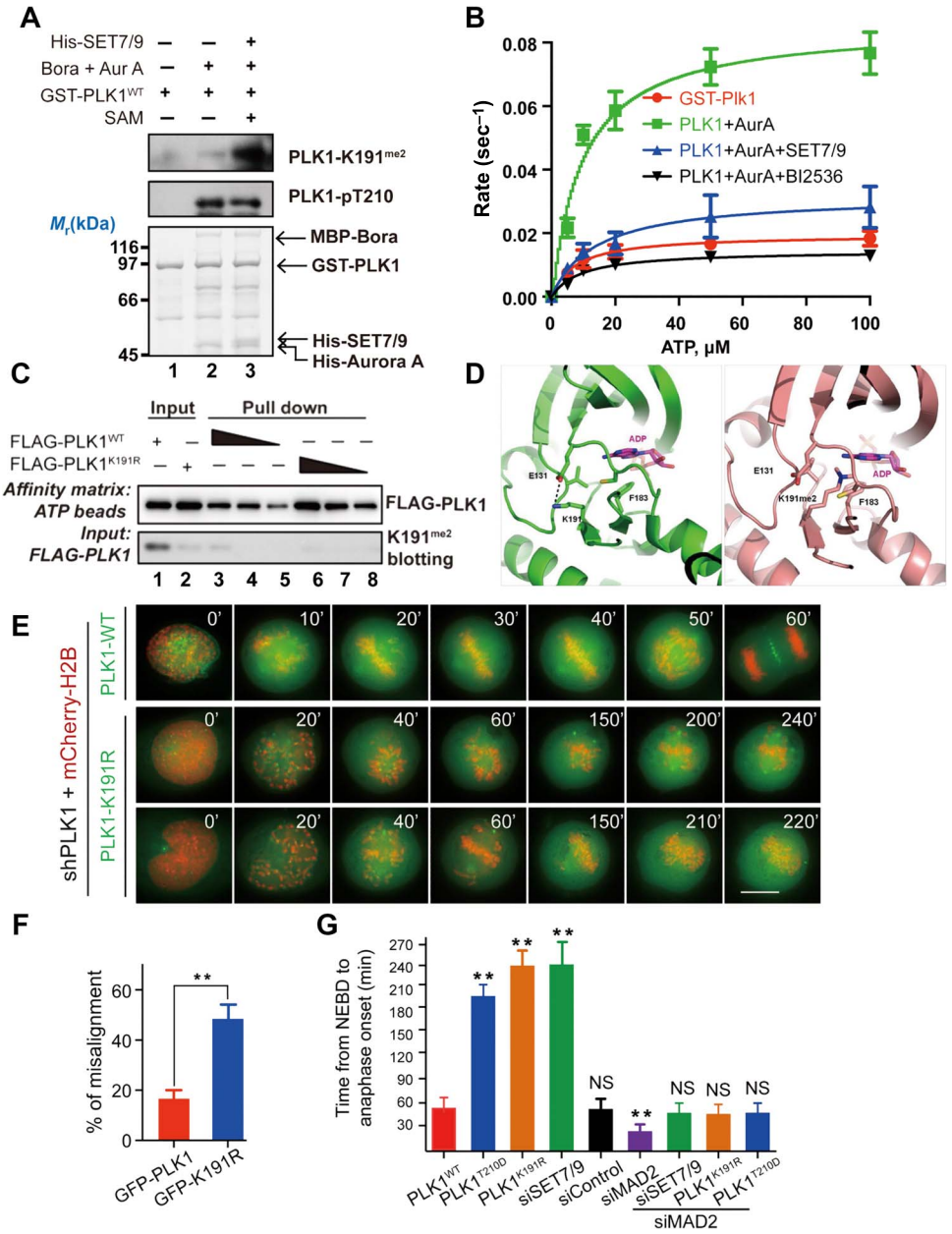

Figure 4 Dimethylation of K191 on PLK1 attenuates its kinase activity. (**A**) GST-PLK1 was incubated with 6× His-tagged Aurora A plus Bora in the presence of 1 mM SAM for *in vitro* methylation assay. The methylation and phosphorylation levels of PLK1 were analyzed by PLK1-K191^{me2} and PLK1-pT210 antibodies, respectively. (**B**) Kinetics of PLK1 (purified as in **A**) kinase activity in the presence of Aurora A and SET7/9 with increased concentration of ATP. Data represent mean ± SEM from three independent experiments. (**C**) FLAG-PLK1^{WT} and FLAG-PLK1^{K191R} were purified from HEK293T cells co-transfected with GFP-SET7/9 and FLAG-PLK1^{WT} or FLAG-PLK1^{K191R}. ATP agarose beads were used as affinity matrices to absorb purified PLK1 with increased amount (0.25–1 μg). The methylation level of PLK1 was analyzed with the anti-PLK1-K191^{me2} antibody. (**D**) Cartoon representation of ADP docked onto PLK1 or dimethylated PLK1 (PLK1-K191^{me2}). Residues for ADP binding are shown as sticks. (**E**) Representative mitotic phenotypes in PLK1-depleted HeLa cells expressing GFP-PLK1^{WT} or GFP-PLK1^{K191R} shown by time-lapse microscopy and visualized with mCherry-H2B. Scale bar, 10 μm. (**F**) Quantification of chromosome misalignment of HeLa cells expressing GFP-PLK1^{WT} (n = 108) or GFP-PLK1^{K191R} (n = 101). Data represent mean ± SEM from three independent experiments. (**G**) Quantification of mitotic duration of PLK1-depleted HeLa cells expressing PLK1^{WT}, PLK1^{T210D}, and PLK1^{K191R} with or without MAD2 depletion. An aliquot of SET7/9 siRNA-treated cells were used as a control. NEBD, nuclear envelope breakdown. At least 103 cells per group were examined from three independent experiments. Data represent mean ± SEM. Statistical significance was tested by two-sided t-test. $^{**}P < 0.01$; NS indicates non-significant, $P > 0.05$.

the dimethylation on K191 extends the side-chain length and hydrophobicity of lysine, which partially occupies the ATP pocket and presents steric hindrance for ATP entry. Thus, we conclude that dimethylation at Lys191 fine-tunes PLK1 activity by limiting ATP utilization.

To examine the functional relevance of Lys191 dimethylation in chromosome segregation, we transfected GFP-PLK1 and non-methylatable GFP-PLK1^{K191R} into HeLa cells expressing mCherry-H2B and depleted of endogenous PLK1 followed by real-time imaging. Interestingly, expression of non-methylatable PLK1 resulted in mitotic arrest in which chromosomes failed to align at the equator (Figure 4F). Consistent with the critical function of PLK1 activity homeostasis, suppression of SET7/9 or persistent activation of PLK1 by expressing PLK1^{T210D} also resulted in mitotic arrest. To examine whether perturbation of PLK1 methylation and elevation of PLK1 activity activated spindle assembly checkpoint, we treated HeLa cells with siRNA targeted to MAD2 and BubR1, respectively, as previously described (Yao et al., 2000; Zhu et al., 2008). The efficiency of siRNA-mediated MAD2 protein suppression was judged by western blotting analyses (Supplementary Figure S4B). As predicted, suppression of MAD2 resulted in mitotic exit in GFP-PLK1^{K191R}-expressing cells and SET7/9-suppressed cells, respectively (Figure 4G). Together, these data suggested that deficiency of SET7/9 activity prevented anaphase onset by persistent activation of SAC via a PLK1-dependent manner. Indeed, our analyses showed that mitotic arrest induced by expression of constitutively active PLK1^{T210D} was reversed by suppression of MAD2 (Figure 4G) or suppression of BubR1 (Supplementary Figure S4C), respectively.

Methylation of Lys191 is essential for homeostatic control of PLK1 activity at kinetochores

It has been recently proposed that PLK1 substrates regulate spindle microtubule stability in mitosis (Zhang et al., 2011; Liu et al., 2013). To examine whether SET7/9-elicited methylation modulates PLK1 kinase activity at kinetochore, we sought to monitor PLK1 activity in kinetochores using FRET-based sensors that report quantitative changes of substrate phosphorylation in live cells (Chu et al., 2011; Liu et al., 2013). Specifically, we adapted a sensor design (Violin et al., 2003), in which changes in intra-molecular FRET between cyan and yellow fluorescent proteins (CFP-YFP) depend on changes in phosphorylation of a PLK1 optimized substrate peptide derived from c-Jun. To mimic localization of endogenous PLK1 substrates (Ruchaud et al., 2007), sensors were targeted to centromeres by fusion to the C terminus of Hec1 (Zhao et al., 2019). To validate the sensor response to changes in PLK1 activity in living cells, we first imaged mitotic cells before and after kinase inhibition as previously reported (Chu et al., 2011, 2012). As shown in Supplementary Figure S5, FRET/CFP emission ratio increased after BI 2536 (a PLK1 inhibitor) treatment, consistent with previous studies (Liu et al., 2009; Chu et al., 2011). Examination of sensor emission ratio revealed that phosphorylation differences between individual kinetochores depend on their position as chromosomes congress to the equator during mitotic progression.

If SET7/9-mediated methylation of PLK1 was a homeostatic regulator for PLK1 activity, suppression of SET7/9 would increase PLK1 activity. As shown in Figure 5A and quantified in Figure 5B, suppression of SET7/9 by siRNA resulted in hyperphosphorylation of the sensor in the kinetochore, supporting the notion that SET7/9 transferase is critical for regulating PLK1 activity in kinetochores. To examine whether PLK1 activity was a function of SET7/9-elicited methylation, we sought to measure kinetochore PLK1 activity in cells expressing wild-type PLK1, PLK1^{K191R}, PLK1^{T210A}, and PLK1^{T210D}. As predicted, expression of mCherry-PLK1^{K191R} resulted in an increase of kinetochore PLK1 kinase activity judged by a decreased sensor emission ratio (Figure 5C). In contrast, expression of mCherry-PLK1^{T210A} increased the sensor emission ratio, demonstrating that kinetochore PLK1 kinase activity is a function of SET7/9-elicited methylation of PLK1.

Consistent with previous analyses (e.g. Figure 4G), suppression of SET7/9 led to an activation of SAC mitotic arrest due to perturbation of PLK1 kinase activity dynamics (Figure 5A, bottom panel). To confirm this, we evaluated the kinetochore localization of BubR1, a key components of the SAC, in SET7/9-depleted cells. In line with the SAC satisfaction, BubR1 staining on kinetochores diminished sharply in control siRNA transfected metaphase cells. In striking contrast, the BubR1 signal was persistently retained on kinetochores in metaphase cells after depletion of SET7/9 (Figure 5D, lower panel). Quantitative analyses of BubR1 signals at the kinetochores of endogenous PLK1-depleted cells expressing PLK1^{K191R} and PLK1^{T210D} demonstrated that increased level of BubR1 retained at the kinetochore is a function of elevated PLK1 activity (Figure 5E), suggesting a critical role of PLK1 activity dynamics in persistent activation of SAC.

Dynamic Lys191 methylation is required for accurate kinetochore-microtubule attachments

Our previous studies show that perturbation of PLK1-mediated phosphorylation of MCAK led to hyperstability of spindle microtubules and hence chromosome segregation defects (Zhang et al., 2011; Shao et al., 2015). To test whether inhibition of PLK1 methylation would result in hyperstabilization of kinetochore microtubules, aliquots of HeLa cells depleted of endogenous PLK1 were transiently transfected with PLK1 targeting to kinetochore using Hec1-PLK1 fusion constructs described previously (Liu et al., 2012). Specifically, Hec1-mCherry-PLK1^{WT}, Hec1-mCherry-PLK1^{K191R}, and Hec1-mCherry-PLK1^{T210D} were introduced into HeLa cells followed by examination of kinetochore microtubule integrity and tension across the sister kinetochore as previously reported (Wang et al., 2012). As shown in Figure 6A, expression of Hec1-mCherry-PLK1^{K191R} and Hec1-mCherry-PLK1^{T210D} but not Hec1-mCherry-PLK1^{WT} resulted in loss of astral microtubules but hyperstabilization of spindle microtubules. If spindle microtubules are hyperstabilized, the sister kinetochore distance should

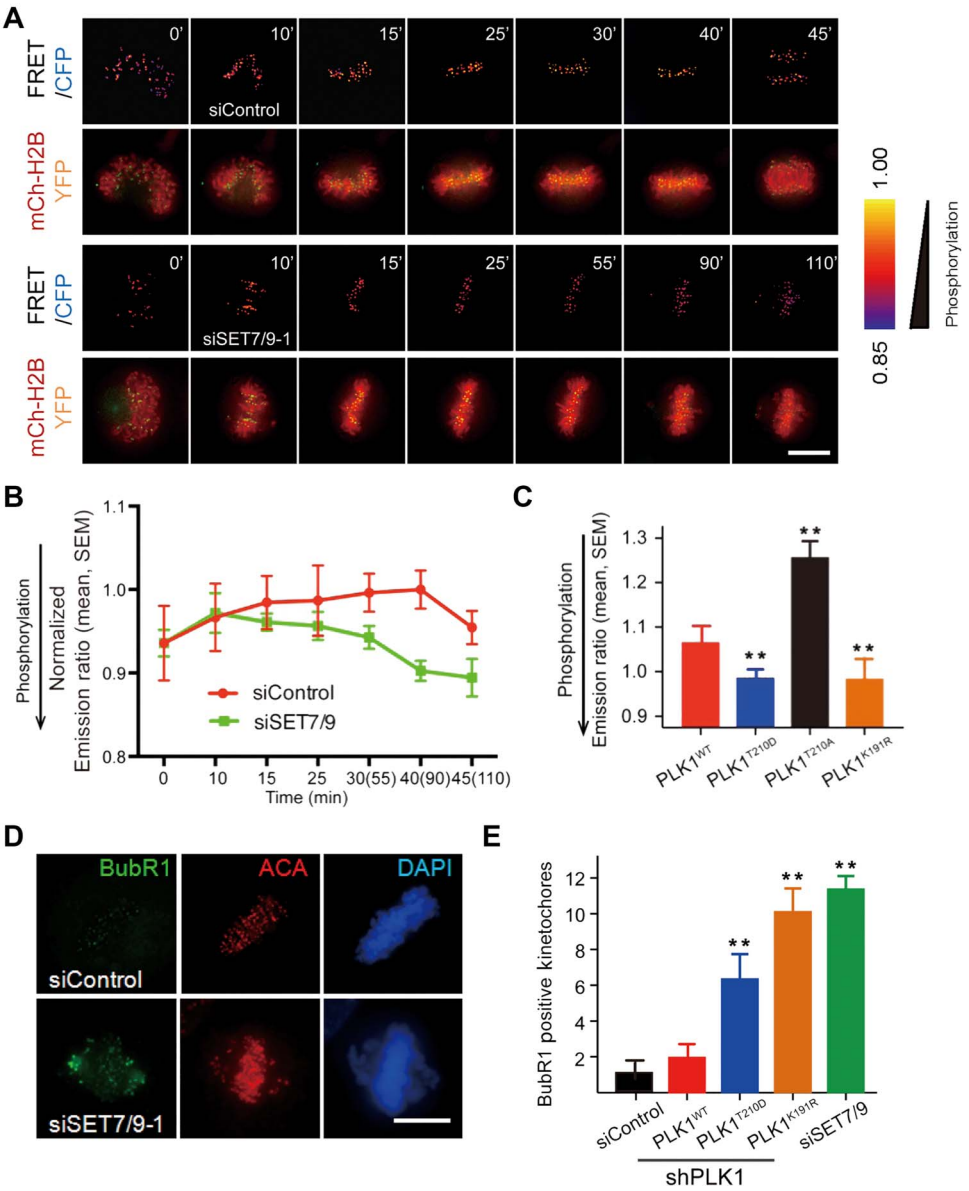

Figure 5 Methylation of PLK1 fine tunes PLK1 kinase activity at kinetochore. (**A**) SET7/9-depleted HeLa cells expressing Hec1-targeted PLK1 kinase sensor were imaged live after 8 h release from thymidine arrest. The first and third panels, color-coded images of the emission ratio; the second and fourth panels, mCherry-H2B (mCh-H2B) merged with YFP signal of the sensor. Note that suppression of SET7/9 resulted in mitotic arrest. Also, the emission ratio decreased drastically when anaphase began due to the localization change of Hec1. Scale bar, 10 μm. (**B**) Statistical analyses of the FRET/CFP emission ratio on centromeres at the indicated time points. Data represent mean ± SEM; > 150 kinetochores of each categories from five different cells. (**C**) Statistical analyses of the FRET/CFP emission ratio of HeLa cells expressing mCherry-PLK1^{WT}, PLK1^{T210D}, PLK1^{T210A}, and PLK1^{K191R}. Non-methylatable PLK1 (PLK1^{K191R}) retained higher PLK1 activity similar to constitutively active PLK1^{T210D}. Data represent mean ± SEM; > 150 kinetochores of each categories from five different cells. (**D**) Representative immunofluorescence images of HeLa cells depleted of SET7/9. Cells were fixed, permeabilized, and stained for anti-BubR1 and ACA antibodies, respectively. Scale bar, 10 μm. (**E**) Statistical analyses of BubR1-positive kinetochores in HeLa cells expressing mCherry-PLK1^{WT}, PLK1^{T210D}, PLK1^{K191R}, and SET7/9 siRNA, respectively. Data represent mean ± SEM from three independent experiments. Statistical significance was tested by two-sided *t*-test. $^{**}P < 0.01$.

reflect a reduced kinetochore tension. Consistently, the average distance between sister kinetochores, judged by Hec1 labelling, is also decreased in Hec1-mCherry-PLK1^{T210D}- and Hec1-mCherry-PLK1^{K191R}-expressing cells (Figure 6B, 0.87 ± 0.04 μm and 0.94 ± 0.03 μm, respectively) than that of Hec1-mCherry-PLK1^{WT}-expressing cells (1.24 ± 0.06 μm), demonstrating a lack of inter-kinetochore tension in the presence of persistent high level of kinetochore-associated PLK1. These data suggests that

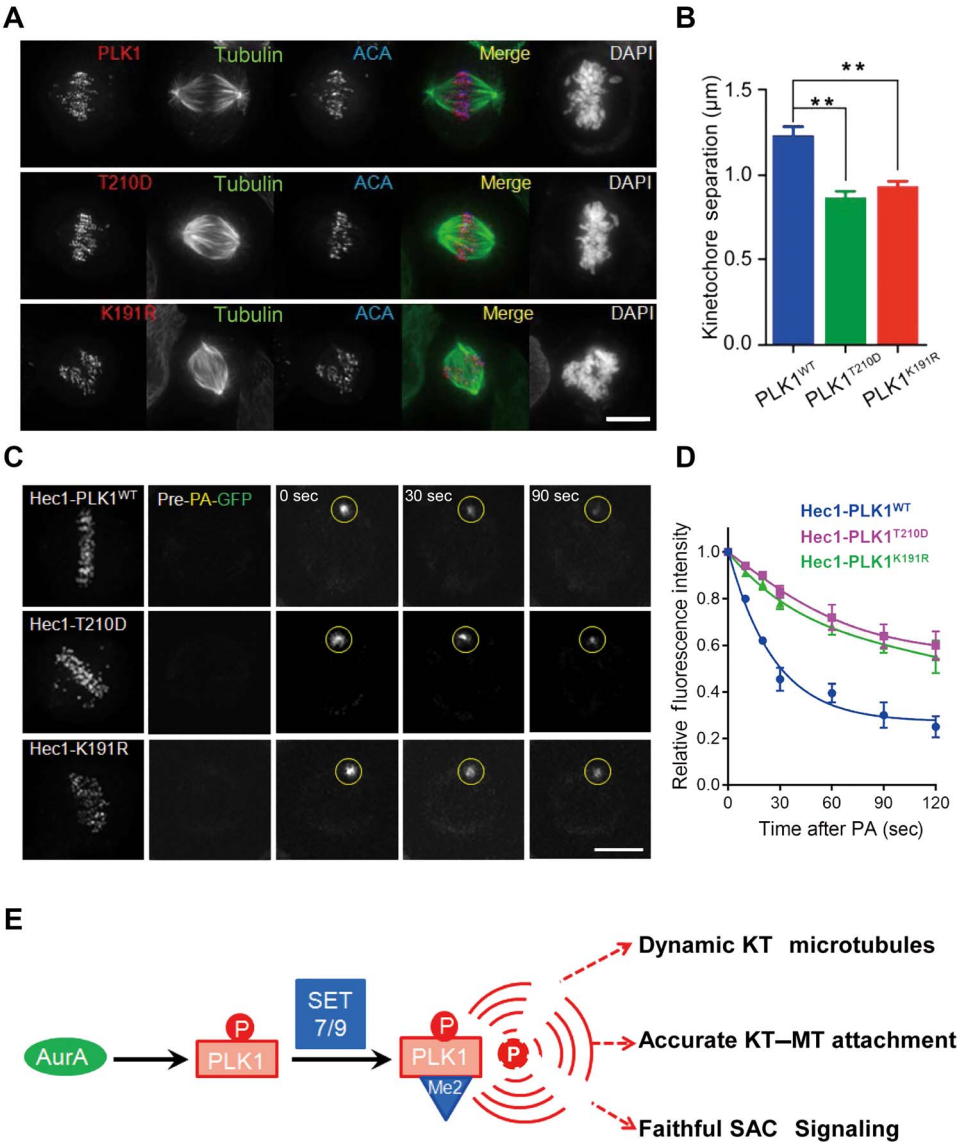

Figure 6 Methylation turns PLK1 activity for dynamic kinetochore microtubule attachments. (**A**) Representative immunofluorescence images of endogenous PLK1-depleted HeLa cells expressing Hec1-mCherry-tagged PLK1^{WT}, PLK1^{T210D}, and PLK1^{K191R}. Transfected cells were fixed, permeabilized, and then stained for anti-α-tubulin and ACA antibodies. Scale bar, 5 μm. (**B**) Statistical analyses of kinetochore distance marked by Hec1 in HeLa cells expressing Hec1-mCherry-tagged PLK1^{WT}, PLK1^{T210D}, and PLK1^{K191R}. Data represent mean ± SEM from three independent experiments. Statistical significance was tested by two-sided *t*-test. $^{**}P < 0.01$. (**C**) Examples of time-lapse confocal images of endogenous PLK1-depleted HeLa cells expressing Hec1-mCherry-tagged PLK1^{WT}, PLK1^{T210D}, and PLK1^{K191R}. Cells were arrested at metaphase and imaged before (Pre-PA) and after photoactivation of GFP-tubulin at indicated time points. Scale bar, 10 μm. (**D**) Statistical analyses of normalized fluorescence intensity over time after photoactivation as in **C** (n = 15 cells for each group). The half-life of photoactivated GFP-tubulin from different groups was then calculated and presented as mean ± SEM. (**E**) Working model accounting for function of PLK1 methylation in accurate kinetochore–microtubule attachment and faithful spindle checkpoint signaling in mitosis.

persistently high PLK1 activity stabilizes spindle microtubules, reduces tension across the sister kinetochore, and perturbs accurate kinetochore-microtubule attachment.

To directly assess whether methylation of kinetochore-associated PLK1 affects microtubule dynamics as cells approach metaphase, we measured microtubule turnover using photoactivatable (PA) GFP-tubulin in cells expressing wild type Hec1-mCherry-PLK1^{WT}, Hec1-mCherry-PLK1^{K191R}, and Hec1-mCherry-PLK1^{T210D} (Wang et al., 2012; Xia et al., 2014). Specifically, a midway between kinetochore and centrosome was photoactivated and the decay of fluorescent spot was followed and quantified as function of time (Figure 6C and D). The decrease in fluorescence after photoactivation is well fitted by a double-exponential curve as previously reported

(Liu et al., 2012; Wang et al., 2012). The half-life of kinetochore microtubule in Hec1-mCherry-PLK1^{T210D}-expressing cells was 2-fold higher than that of Hec1-mCherry-PLK1^{WT}-expressing cells, while the half-life of kinetochore microtubule in Hec1-mCherry-PLK1^{K191R}-expressing cells is similar to that of Hec1-mCherry-PLK1^{T210D}-expressing cells. These results show that persistent increase of PLK1 activity at kinetochores as expressing Hec1-mCherry-PLK1^{T210D} suppresses microtubule dynamics, consistent with our findings of reduced inter-kinetochore tension and the literature (Zhang et al., 2011; Liu et al., 2012). Inhibition of PLK1 methylation at the kinetochore as expressing Hec1-mCherry-PLK1^{K191R} also suppresses microtubule dynamics (Figure 6D), indicating that SET7/9 synergizes with kinetochore PLK1 to promote spindle microtubule dynamics. Thus, we conclude that methylation of PLK1 at kinetochore by SET7/9 provides a homeostatic control of PLK1 activity in space and time.

Discussion

Kinetochores are specialized protein machines involved in maintaining genomic stability during mitosis by orchestrating accurate chromosome-microtubule attachments and SAC. Synergistic action of Bora and the Aurora A kinase controls the G2-M transition by phospho-activation of PLK1, leading to the activation of CDK1 and mitotic entry. Methylation of PLK1 by SET7/9 therefore provided homeostatic regulation of PLK1 at kinetochore for accurate attachment of spindle microtubules before sister chromatid separation. Our identification of the SET7/9–PLK1 signaling axis uncovered a new regulatory mechanism by which methylation of PLK1 prevented Aurora A-mediated hyperphosphorylation of T-loops to fine tune the activity of PLK1 for control of chromosome stability (Figure 6E). It would be of great interest, in follow-up studies, to characterize additional substrates of SET7/9 in kinetochore and delineate their precise molecular function in mitosis.

We identified a molecular mechanism involving SET7/9–PLK1 axis that underlies kinetochore sensing of aberrant microtubule attachment and established its connection to error-free metaphase-anaphase transition, as perturbation of the axis gave rise to premature anaphase. Our study highlighted how a methylation–phosphorylation cascade senses and avoids hyperstabilized chromosome attachment during mitosis to maintain genomic stability. During the preparation of this work, two studies reported PLK1 methylation at different sites. One study showed that SETD6 methylates PLK1 at K209 and K413 which keep mitosis in check and deficiency of SETD6 activity promotes cellular proliferation (Feldman et al., 2019). The second study described that PLK1 activity is controlled by methyltransferase G9a at Lys209 (Li et al., 2019), which antagonizes phosphorylation of T210 to inhibit PLK1 activity, and all these three sites are labelled in Supplementary Figure S3B. Since the methyl-deficient mutant K209A affects DNA replication, it is likely that Lys209 methylation is a switch for PLK1 function in DNA damage repair. The fact that Lys191 is evolutionarily conserved from yeast to human suggest a functional conservation of Lys191 as an essential fitness machinery in eukaryotic cell division control while other two methylation sites may exhibit context-dependent regulation. It would be of great interest in the future studies to model the methylation site-specific function using physiological system such as organoids (Liu et al., 2019; Yao and Smolka, 2019). Our present study delineated SET7/9 function in mitosis in which SET7/9-elicited methylation of PLK1 orchestrated phosphorylation kinetics at kinetochore for accurate chromosome alignment and segregation. Collectively, these three studies on PLK1 methylation shed light on how PLK1 methylation serves as a genomic guardian in orchestrating chromatin plasticity during DDR processes and establishing proper kinetochore-microtubule attachment for error-free metaphase-anaphase transition in mitosis (Figure 6E). It would be of great interest to ascertain the respective function of Lys191, Lys209, and Lys413 in regulating spindle microtubule dynamics and plasticity during cell division.

Our present study delineates the cellular function of SET7/9 in mitosis but not earlier events by which SET7/9-elicited inhibition of PLK1 orchestrated activity of PLK1 at the kinetochores for accurate chromosome alignment and segregation. These results explain how methylation of PLK1 serves as a genome guardian by orchestrating chromatin plasticity during DDR processes and generating an optimal PLK1 activity for stable kinetochore attachment and error-free metaphase–anaphase transition in mitosis via a methyl-phosphorylation crosstalk. Future study should explore whether there are other lysine modifications such as acetylation on Lys191 in a context-dependent manner during cell division control (Bao et al., 2018; Liu et al., 2018). In addition, it would be of great interest to delineate the spatiotemporal dynamics of Lys191 methylation relative to those two other methylation sites (Feldman et al., 2019; Li et al., 2019).

Together with our findings that SUV39H1 generates a methylation gradient at kinetochore that provides a spatiotemporal cue for accurate chromosome segregation in mitosis (Chu et al., 2012) and synergism between SUV39H1 and SET7/9, this work provides a unifying view of a previously uncharacterized molecular mechanism that underlies methyl regulation in mitosis and defines a signaling axis that integrates protein phosphorylation and methylation to connect cell cycle progression with genomic stability.

Materials and methods

Cell culture, synchronization, and transfection

HeLa cells and HEK293T cells (American Type Culture Collection) were cultured in DMEM (Gibco) with 10% (*v*/*v*) FBS (HyClone) and penicillin–streptomycin (100 units/ml and 100 µg/ml, respectively; Gibco) at 37°C in a humidified atmosphere with 8% CO_2. For cell cycle synchronization, HeLa cells were first blocked in G1/S with 2.5 mM thymidine (Sigma) for 16 h and then released in fresh culture medium for 8 h to enrich mitotic cells. For some experiments, 20 µM MG132 was added to synchronize cells at metaphase.

Plasmids

To generate GFP-tagged and Flag-tagged full-length PLK1 and its deletion mutants, PCR-amplified PLK1 cDNA or fragments were cloned into the pEGFP-C1 vector (Clontech) and 3× FLAG-Myc-CMV-24 vector (Sigma) by ClonExpress Entry One Step Cloning Kit (Vazyme). Site-specific mutants of FLAG- and EGFP-tagged PLK1 were generated by ClonExpress Entry One Step Cloning Kit (Vazyme). To generate MBP-Bora, GFP-Bora was amplified by PCR and cloned into PMAL-C2X vector. GST-3×MBT was kindly provided by Dr Stephen D. Nimer (University of Miami). Hec1-PLK1 FRET sensor was generated as reported previously (Chu et al., 2012). His-SET7/9 was purchased from Addgene.

To test the significance of kinetochore-associated PLK1 activity in response to SET7/9 methylation during mitosis, we designed a strategy to constitutively target PLK1 to kinetochores by fusing the kinase to Hec1 as previously reported (Liu et al., 2012). Specifically, Hec1-mCherry-PLK1^{WT}, Hec1-mCherry-PLK1^{K191R}, and Hec1-mCherry-PLK1^{T210D} fusion constructs were generated and validated by DNA sequencing.

siRNA transfection and drug treatment

HeLa cells grown to 40% confluence on 150-mm^2 culture flasks at 37°C with 8% (*v*/*v*) CO_2 were transfected with different siRNAs using RNAiMAX (Invitrogen) or shRNAs using Lipofectamine 3000 (Invitrogen). siSET7/9-1 (5′-GGGCACCUGGACGAUGACGGA-3′), siSET7/9-2 (5′-GCCUUGUAGGAGAAGUAAA-3′), siMad2 (5′-UCCGUUCAGUGAUCAGACA-3′), siBubR1 (5′-GUCUCACAGAUU-GCUGCCU-3′), and siControl (5′-UAAAUGUACUGCGCGUGGAGAGG AA-3′) were synthesized from Qiagen. PLK1 shRNA targeting the 3′-UTR (5′-CCGGAGCTGCATCATCCTTGCAGGTCTCGAGACCTGCAAG GATGATGCAGCTTTTTT-3′) of PLK1 gene was purchased from Sigma-Aldrich (TRCN0000011006).

Nocodazole (100 ng/ml, ≥99%), monastrol (50 μM, ≥98%), MG132 (10 μM, ≥90%), PFI-2 (10 μM, ≥97%), cyproheptadine (2 μM, ≥99%), and S-(5′-adenosyl)-L-methionine (SAM, 1 mM, ≥80%) were from Sigma.

Antibodies

The following antibodies were used: anti dimethylated lysine antibody (Abcam; ab23366), anti-FLAG mouse antibody (M2; Sigma-Aldrich; F1804), anti-α-tubulin mouse antibody (DM1A; Sigma-Aldrich; T9026), anti-GFP mouse antibody (GFP-20; Sigma; G6539), anti-PLK1-pT210 mouse antibody (BD; 558400), anti-PLK1 mouse antibody (Invitrogen; 377000), anti-Cyclin B1 antibody (CalBiochem; CC03), anti-BubR1 mouse antibody (BD Biosciences; 612502), and anti-SET7/9 rabbit antibody (Santa Cruz; sc-56774). ACA is a generous gift from Dr Don Cleveland (University of California, San Diego). Anti-dimethylated K191-PLK1 rabbit antibody (PLK1-K191^{me2}) was generated by YenZym LLC. To generate this antibody, a synthetic peptide containing chemically dimethylated K191 (*C*-FLNEDLEV-K*me2*-IGDFG) was conjugated to rabbit albumin (Sigma) and injected into rabbits as previously described (Yao et al., 2000). Serum was collected by a standard protocol and preabsorbed by unmethylated PLK1 peptide (*C*-FLNEDLEVIGDFG) followed by affinity-purification using (*C*-FLNEDLEV-K*me2*-IGDFG)-conjugated divinyl sulfone Sepharose beads (Sigma). The IgG reacting dimethylated K191 was purified and characterized as previously reported (Mo et al., 2016).

Recombinant protein preparation

The plasmids of GST-fusion, MBP-tagged or 6× His-tagged proteins were transformed into *E. coli* strain BL21 or Rosetta (DE3), and expression was induced with 0.5 mM IPTG, with shaking overnight at 16°C. Bacteria expressing GST-SET7/9 and GST-PLK1 (WT, K191R, K474R/K492R) were suspended and lysed by sonication in PBS buffer containing protease inhibitor cocktail (Sigma; P8849) and 1 μg/ml PMSF, followed by purification using glutathione-Sepharose 4B (Sigma).

Bacteria expressing MBP-Bora were suspended and lysed by sonication in MBP column buffer (20 mM Tris–HCl, pH 7.4, 200 mM NaCl, 1 mM EDTA) containing protease inhibitor cocktail (Sigma; P8849) plus 1 μg/ml PMSF, followed by use of amylose resin, as described previously (Seki et al., 2008).

Bacteria expressing 6×His-PLK1 were suspended and lysed by sonication in lysis buffer (50 mM NaH_2PO_4, pH 8.0, 150 mM NaCl, 10 mM imidazole) with protease inhibitor cocktail (Sigma; P8849) and 1 μg/ml PMSF. Then 6× His-tagged proteins were bound to Ni-NTA resin (Qiagen) and eluted with elution buffer (50 mM NaH_2PO_4, pH 8.0, 150 mM NaCl, 200 mM imidazole). All purified proteins were analyzed and confirmed by SDS–PAGE.

GST pull-down assays

GST or GST-tagged proteins immobilized on agarose beads were incubated with cell lysates or purified proteins in PBS buffer at 4°C for 3 h. The resins were washed three times with PBS buffer containing 0.05% Triton X-100 and once with PBS buffer, followed by boiling in SDS–PAGE buffer. The samples were subjected to SDS–PAGE and detected by western blots. MBT pull-downs were performed as previously described (Carlson et al., 2014).

Immunoprecipitation

For immunoprecipitation, HeLa cells were synchronized with nocodazole and collected by shaking off, and then lysed in lysis buffer (50 mM Tris-HCl, pH 8.0, 120 mM NaCl, 0.5% NP-40) supplemented with protease inhibitor cocktail (Sigma) and phosphatase inhibitor cocktail (Sigma). After pre-clearing with Protein A/G resin, the lysate was incubated with PLK1 antibody at 4°C for 24 h with gentle rotation. Protein A/G resin was then added to the lysates, and they were incubated for another 6 h. The Protein A/G resin was then spun down and washed five times with lysis buffer before being resolved by SDS–PAGE and immunoblotted with the indicated antibodies. For FLAG-tagged protein immunoprecipitation, the FLAG-M2 resin was added to the lysates and incubated for 4 h before washing.

Characterization of PLK1 kinetics

Cells co-transfected with GFP-SET7/9 and FLAG-PLK1^{WT} or FLAG-PLK1^{K191R} were extracted in lysis buffer (50 mM HEPES, pH 7.4, 1 mM $MgCl_2$, 1 mM EGTA, 0.5% Triton X-100, 1 mM NaF, 1 mM Na_3VO_4, protease inhibitors) and incubated for 2 h at 4°C with FLAG-M2 beads. Immuno-isolated complexes were eluted by 3× FLAG peptides and quantified by CBB staining. Kinetic parameters were measured by Amplite^{TM} Universal Fluorimetric Kinase Assay Kit (AAT Bioquest, Inc.) as previously described (Huang et al., 2019). Briefly, PLK1 kinase was incubated with Cep55 peptides in 20 µl kinase buffer (20 mM Tris-HCl, pH 7.5, 10 mM $MgCl_2$) in the presence of 0–100 µM ATP for 30 min at 37°C. ADP sensor and sensor buffer were added into the preparations, which were incubated for another 15 min at room temperature. The amount of ADP produced from the kinase reaction was detected by monitoring fluorescence intensity at Ex/Em = 540/590 nm on TECAN Genios Plus. K_m and k_{cat} values were calculated according to the Michaelis–Menten equation. The sequence of Cep55 peptide is PKSPTAALNESLVECPKCNIQ.

In vitro phosphorylation assay

Aurora A kinase (Invitrogen; PV3612) were incubated with PLK1 (with or without GST-fusion or 6× His-tagged) at 30°C for 30 min in a final volume of 30 µl containing 20 mM Tris, pH 7.4, 10 mM $MgCl_2$, 1 mM ATP, and 1 mM DTT. Reactions were stopped by adding 5× SDS sample buffer and boiled at 100°C for 5 min. Samples were resolved by SDS–PAGE and visualized by western blot.

In vitro methylation assay

The recombinant His-SET7/9 and GST-PLK1^{WT} or GST-PLK1^{K191R} proteins were purified and incubated in *in vitro* methyl buffer (50 mM Tris–HCl, 100 mM NaCl, and 1 mM DTT, pH 8.0) with or without 1 mM SAM at 25°C. The reaction was terminated by SDS–PAGE sample buffer and protein samples were subjected to western blotting.

Immunofluorescence

HeLa cells grown on coverslips were permeabilized with PHEM buffer (100 mM PIPES, pH 6.8, 20 mM HEPES, 5 mM EGTA, 2 mM $MgCl_2$) containing 0.2% Triton X-100 at 37°C for 1 min and fixed in 3.7% paraformaldehyde in PHEM at 37°C for 5 min as previously reported (Yao et al., 1997). Then, the samples were processed for indirect immunofluorescence microscopy. Immunofluorescence images were collected under a DeltaVision wide-field deconvolution microscope system (Applied Precision Inc.) as previously described (Yao et al., 2000). Z-series stacks were obtained at 0.45 µm steps using a 60×/NA 1.4 Plan Apochromat objective (Olympus) with 1 × 1 binning. Images were deconvolved using SoftWoRx (Applied Precision) and processed with ImageJ. The distance between sister kinetochores marked with ACA was measured as described previously (Liu et al., 2007, 2012).

Fluorescence intensity quantification

Quantification of the BubR1-positive kinetochore was conducted as described (Yao et al., 2000; Liu et al., 2007). In brief, the average pixel intensities of BubR1 marked kinetochore from at least 50 centromere pairs from five cells were measured, and background pixel intensities were subtracted. The pixel intensities of BubR1 at each kinetochore pair were then normalized against ACA pixel values to account for any variations in staining or image acquisition. The BubR1 positive kinetochores were then plotted as a reporter of misaligned kinetochore from cells transfected with a control and SET7/9 siRNA duplex.

Kinetochore distance measurement

The distance between sister kinetochores marked with ACA was measured as the distance between the peak fluorescence as described previously (Yao et al., 2000). When suitable kinetochore pairs were identified, the image was enlarged 3-fold to facilitate accurate placement of a computer-generated cursor over the center of each kinetochore. Only sister kinetochores that were in the same focal plane were measured.

Live cell imaging

Live cell imaging was performed as described previously (Xia et al., 2012; Mo et al., 2016). HeLa cells were cultured in CO_2-independent medium plus 10% FBS and 2 mM glutamine at 37°C. Cells expressing mCherry-H2B and GFP-tubulin were transfected with the indicated siRNA(s) and synchronized. In some cases, wild-type, constitutively active (T210D), and non-methylatable PLK1 (K191R) mutants were transfected with siRNA into HeLa cells, respectively, followed by synchronization. Images were acquired from nuclear envelope breakdown with 3- or 5-min intervals for mitotic process by a DeltaVision deconvolution microscope system built on an Olympus IX-71 inverted microscope base (Applied Precision). For imaging, a 60× 1.42 NA lens was used, and optical sections were taken at intervals of 0.4 µm. Images for display were generated by projecting single optical sections and prepared for publication using Adobe Photoshop software.

FRET assay

For FRET assay, HeLa cells expressing various PLK1 constructs and mCherry-H2B were synchronized with thymidine as previously reported (Chu et al., 2011, 2012). Transfected cells grown on glass-based dishes (IWAKI) were supplemented with CO_2-independent medium (Gibco) and observed using the DeltaVision RT system (Applied Precision) at a temperature of 37°C. The images were taken at 5-min intervals with an exposure time of 0.1 sec. For live cell imaging of FRET sensor, CFP was excited at 470 nm, and CFP and YFP emissions were acquired simultaneously with a beam splitter (Dual-View, Optical Insights). Individual centromeres or kinetochores were defined automatically from confocal image stacks, and the YFP/CFP or FRET/CFP emission ratio was calculated at each centromere/kinetochore as previously described (Chu et al., 2011, 2012).

GFP-tubulin photoactivation in live mitosis

GFP-tubulin photoactivation was performed as described previously (Wang et al., 2012). Briefly, HeLa cells were grown on a glass bottom culture dish (MatTek) at 37°C after transfection with PLK1 shRNA. HeLa cells were transiently transfected with PA-GFP-tubulin and Hec1-mCherry-PLK1 wild-type or non-methylatable mutant followed by synchronization, and then mitotic cells were identified by DIC microscopy. Several pulses from a 405-nm diffraction-limited laser on LSM710 NLO (Carl Zeiss) were used to photoactivate an area of $< 2\ \mu m^2$ within the spindle. Images were acquired with 63×, 1.4 numerical aperture objectives on a LSM710 laser-scanning microscope, and images were collected every 10 sec. The fluorescence intensity of photoactivated region was analyzed with ImageJ and Zeiss Zen software as described previously (Wang et al., 2012; Xia et al., 2014).

Statistics

All statistics are described in the figure legends. Two-sided unpaired Student's *t* test was applied for experimental comparisons, using GraphPad Prism. All western blotting analyses were taken from three separated experiments. No statistical method was used to predetermine sample size. All data were expected to have normal distribution.

Acknowledgements

We are grateful to Drs Stephen D. Nimer and Dan Liu for reagents. We thank all the members of our laboratories for insightful discussion and suggestions.

Funding

This work was supported in part by the National Natural Science Foundation of China (31430054, 31320103904, 31621002, 31671405, 91854203, 91853115, 21922706, 31671407, 31871359, 31601097, and 21672201), the National Key Research and Development Program of China (2017YFA0503600 and 2016YFA0100500), 'Strategic Priority Research Program' of the Chinese Academy of Sciences (XDB19000000), Chinese Academy of Sciences Center for Excellence in Molecular Cell Science (2015HSC-UE010), MOE Innovative Team (IRT_17R102), and the US National Institutes of Health (CA164133 and DK26929).

Conflict of interest: none declared.

Author contributions

X.Y. and X.L. conceived the project. R.Y. and H.W. designed and performed most cell biology experiments. R.Y., H.W., F.Y., H.I., T.W., P.G., M.A., S.D., J.C., Y.C., and F.M. designed and performed biochemical experiments. Q.W., and M.Y. performed mass spectrometry analysis. R.Y., H.W., W.W., J.W., X.G., Z.D., and X.L. performed data analyses. Y.Z., G.F., and P.R.C. contributed to reagents. All authors contributed to the writing or editing of the manuscript.

References

Akram, S., Yang, F., Li, J., et al. (2018). LRIF1 interacts with HP1α to coordinate accurate chromosome segregation during mitosis. J. Mol. Cell Biol. *10*, 527–538.

Bao, X., Liu, H., Liu, X., et al. (2018). Mitosis-specific acetylation tunes Ran effector binding for chromosome segregation. J. Mol. Cell Biol. *10*, 18–32.

Barsyte-Lovejoy, D., Li, F., Oudhoff, M.J., et al. (2014). (R)-PFI-2 is a potent and selective inhibitor of SETD7 methyltransferase activity in cells. Proc. Natl Acad. Sci. USA *111*, 12853–12858.

Campaner, S., Spreafico, F., Burgold, T., et al. (2011). The methyltransferase Set7/9 (Setd7) is dispensable for the p53-mediated DNA damage response in vivo. Mol. Cell *43*, 681–688.

Carlson, S.M., Moore, K.E., Green, E.M., et al. (2014). Proteome-wide enrichment of proteins modified by lysine methylation. Nat. Protoc. *9*, 37–50.

Chu, L., Zhu, T., Liu, X., et al. (2012). SUV39H1 orchestrates temporal dynamics of centromeric methylation essential for faithful chromosome segregation in mitosis. J. Mol. Cell Biol. *4*, 331–340.

Chu, Y., Yao, P.Y., Wang, W., et al. (2011). Aurora B kinase activation requires survivin priming phosphorylation by PLK1. J. Mol. Cell Biol. *3*, 260–267.

Cleveland, D.W., Mao, Y., and Sullivan, K.F. (2003). Centromeres and kinetochores: from epigenetics to mitotic checkpoint signaling. Cell *112*, 407–421.

Duan, H., Wang, C., Wang, M., et al. (2016). Phosphorylation of PP1 regulator Sds22 by PLK1 ensures accurate chromosome segregation. J. Biol. Chem. *291*, 21123–21136.

Esteve, P.O., Chin, H.G., Benner, J., et al. (2009). Regulation of DNMT1 stability through SET7-mediated lysine methylation in mammalian cells. Proc. Natl Acad. Sci. USA *106*, 5076–5081.

Feldman, M., Vershinin, Z., Goliand, I., et al. (2019). The methyltransferase SETD6 regulates mitotic progression through PLK1 methylation. Proc. Natl Acad Sci. USA *116*, 1235–1240.

Fu, L., Wu, H., Cheng, S.Y., et al. (2016). Set7 mediated Gli3 methylation plays a positive role in the activation of Sonic Hedgehog pathway in mammals. eLife *5*, pii: e15690.

Golsteyn, R.M., Mundt, K.E., Fry, A.M., et al. (1995). Cell cycle regulation of the activity and subcellular localization of Plk1, a human protein kinase implicated in mitotic spindle function. J. Cell Biol. *129*, 1617–1628.

Hirano, T., Fujiwara, T., Niwa, H., et al. (2018). Development of novel inhibitors for histone methyltransferase SET7/9 based on cyproheptadine. ChemMedChem *13*, 1530–1540.

Huang, J., Perez-Burgos, L., Placek, B.J., et al. (2006). Repression of p53 activity by Smyd2-mediated methylation. Nature *444*, 629–632.

Huang, Y., Lin, L., Liu, X., et al. (2019). BubR1 phosphorylates CENP-E as a switch enabling the transition from lateral association to end-on capture of spindle microtubules. Cell Res. *29*, 562–578.

Kalakonda, N., Fischle, W., Boccuni, P., et al. (2008). Histone H4 lysine 20 monomethylation promotes transcriptional repression by L3MBTL1. Oncogene *27*, 4293–4304.

Ke, Y.W., Dou, Z., Zhang, J., et al. (2003). Function and regulation of Aurora/Ipl1p kinase family in cell division. Cell Res. *13*, 69–81.

Kontaki, H., and Talianidis, I. (2010). Lysine methylation regulates E2F1-induced cell death. Mol. Cell *39*, 152–160.

Li, W., Wang, H.Y., Zhao, X., et al. (2019). A methylation-phosphorylation switch determines Plk1 kinase activity and function in DNA damage repair. Sci. Adv. *5*, eaau7566.

Liu, D., Davydenko, O., and Lampson, M.A. (2012). Polo-like kinase-1 regulates kinetochore-microtubule dynamics and spindle checkpoint silencing. J. Cell Biol. *198*, 491–499.

Liu, D., Ding, X., Du, J., et al. (2007). Human NUF2 interacts with centromere-associated protein E and is essential for a stable spindle microtubule-kinetochore attachment. J. Biol. Chem. *282*, 21415–21424.

Liu, D., Vader, G., Vromans, M.J., et al. (2009). Sensing chromosome bi-orientation by spatial separation of aurora B kinase from kinetochore substrates. Science *323*, 1350–1353.

Liu, Q.R., Yan, X.M., Guo, L., et al. (2018). AMPK regulates anaphase central spindle length by phosphorylation of KIF4A. J. Mol. Cell Biol. *10*, 2–17.

Liu, X., Xu, L., Li, J., et al. (2019). Mitotic motor CENP-E cooperates with PRC1 in temporal control of central spindle assembly. J. Mol. Cell Biol. doi: 10.1093/jmcb/mjz051.

Liu, Z., Ren, J., Cao, J., et al. (2013). Systematic analysis of the Plk-mediated phosphoregulation in eukaryotes. Brief. Bioinform. *14*, 344–360.

Mo, F., Zhuang, X., Liu, X., et al. (2016). Acetylation of Aurora B by TIP60 ensures accurate chromosomal segregation. Nat. Chem. Biol. *12*, 226–232.

Nishioka, K., Chuikov, S., Sarma, K., et al. (2002). Set9, a novel histone H3 methyltransferase that facilitates transcription by precluding histone tail modifications required for heterochromatin formation. Genes Dev. *16*, 479–489.

Park, I.Y., Powell, R.T., Tripathi, D.N., et al. (2016). Dual chromatin and cytoskeletal remodeling by SETD2. Cell *166*, 950–962.

Rajagopalan, H., and Lengauer, C. (2004). Aneuploidy and cancer. Nature *432*, 338–341.

Ruchaud, S., Carmena, M., and Earnshaw, W.C. (2007). The chromosomal passenger complex: one for all and all for one. Cell *131*, 230–231.

Seki, A., Coppinger, J.A., Jang, C.Y., et al. (2008). Bora and the kinase Aurora a cooperatively activate the kinase Plk1 and control mitotic entry. Science *320*, 1655–1658.

Shao, H., Huang, Y., Zhang, L., et al. (2015). Spatiotemporal dynamics of Aurora B–PLK1–MCAK signaling axis orchestrates kinetochore bi-orientation and faithful chromosome segregation. Sci. Rep. *5*, 12204.

Takaki, T., Trenz, K., Costanzo, V., et al. (2008). Polo-like kinase 1 reaches beyond mitosis—cytokinesis, DNA damage response, and development. Curr. Opin. Cell Biol. *20*, 650–660.

Violin, J.D., Zhang, J., Tsien, R.Y., et al. (2003). A genetically encoded fluorescent reporter reveals oscillatory phosphorylation by protein kinase C. J. Cell Biol. *161*, 899–909.

Wang, J., Hevi, S., Kurash, J.K., et al. (2009). The lysine demethylase LSD1 (KDM1) is required for maintenance of global DNA methylation. Nat. Genet. *41*, 125–129.

Wang, X., Zhuang, X., Cao, D., et al. (2012). Mitotic regulator SKAP forms a link between kinetochore core complex KMN and dynamic spindle microtubules. J. Biol. Chem. *287*, 39380–39390.

Xia, P., Liu, X., Wu, B., et al. (2014). Superresolution imaging reveals structural features of EB1 in microtubule plus-end tracking. Mol. Biol. Cell *25*, 4166–4173.

Xia, P., Wang, Z., Liu, X., et al. (2012). EB1 acetylation by P300/CBP-associated factor (PCAF) ensures accurate kinetochore-microtubule interactions in mitosis. Proc. Natl Acad. Sci. USA *109*, 16564–16569.

Yang, Y., Wu, F., Ward, T., et al. (2008). Phosphorylation of HsMis13 by Aurora B kinase is essential for assembly of functional kinetochore. J. Biol. Chem. *283*, 26726–26736.

Yao, X., Abrieu, A., Zheng, Y., et al. (2000). CENP-E forms a link between attachment of spindle microtubules to kinetochores and the mitotic checkpoint. Nat. Cell Biol. *2*, 484–491.

Yao, X., Anderson, K.L., and Cleveland, D.W. (1997). The microtubule-dependent motor centromere-associated protein E (CENP-E) is an integral component of kinetochore corona fibers that link centromeres to spindle microtubules. J. Cell Biol. *139*, 435–447.

Yao, X., and Smolka, A. (2019). Gastric parietal cell physiology and Helicobacter pylori-induced disease. Gastroenterology *156*, 2158–2173.

Zhang, L., Shao, H., Huang, Y., et al. (2011). PLK1 phosphorylates mitotic centromere-associated kinesin and promotes its depolymerase activity. J. Biol. Chem. *286*, 3033–3046.

Zhao, G., Cheng, Y., Gui, P., et al. (2019). Dynamic acetylation of the kinetochore-associated protein HEC1 ensures accurate microtubule-kinetochore attachment. J. Biol. Chem. *294*, 576–592.

Zhu, M., Wang, F., Yan, F., et al. (2008). Septin 7 interacts with CENP-E and is required for its kinetochore localization. J. Biol. Chem. *283*, 18916–18925.